

Simulation of pyrolysis gas within a thermal protection system

Alexandre Martin* and Iain D. Boyd†

Department of Aerospace Engineering, University of Michigan, Ann Arbor, MI, 48109, USA

As the first part of an ongoing study on heat flux and ablation on hypersonic vehicles, a material response implicit solver with solid ablation and pyrolysis is developed. As a first step, code-to-code validations and comparisons with experimental data are performed. A study of the various effects of pyrolysis gas within an ablator is also performed; using realistic re-entry conditions on a generic carbon-phenolic ablator, conditions for non-Darcian behavior are modeled, suggesting the use of Forchheimer's Law to calculate gas velocity. The necessary conditions required for kinetic energy to be relevant are also highlighted. The code is then coupled to LeMANS, a CFD solver for the simulation of weakly ionized hypersonic flows in thermo-chemical non-equilibrium developed at The University of Michigan. A summary of the coupling validation is presented. All results show good agreement with published numerical results or analytical solutions.

Nomenclature

Symbols

A	Area	\dot{s}	Recession velocity
b	Permeability slip parameter	St	Stanton number for heat transfer
B'	Non-dimensionalized blowing rate	t	Time
C_e	Heat transfer coefficient; $C_e = \rho_e u_e St$	T	Temperature
E	Total energy	T_v	Vibrational temperature
f	Blasius function	u, v	Velocity
Fo	Forchheimer number	v'	Superficial velocity; $v' = \phi v$
h	Enthalpy	V	Volume
H_r	Recovery enthalpy	x, y	Coordinates
K	Permeability	Y_i	Species mass fraction
K_0	Continuum flow permeability	β	Forchheimer coefficient
\dot{m}'''	Volumetric mass source term	β_K	Ergun's inertial parameter
\dot{m}	Mass flux	η	Blasius coordinate
p	Pressure	λ	Blowing correction fitting parameter
p_η	Conserved pressure in the normal direction	μ	Dynamic viscosity
\dot{q}''	Internal heat flux	Ω	Heat flux correction
q	Surface heat transfer rate	ρ	Density
R	Specific gas constant	ϕ	Porosity
Re	Reynolds Number		
Re _x	Local Reynolds Number		

Subscripts

*Postdoctoral Research Associate, AIAA Member.

†Professor, Associate Fellow AIAA.

0	Non blowing	<i>nc</i>	Neighboring cell
<i>c</i>	Char	<i>s</i>	Solid
<i>cv</i>	Control volume	<i>st</i>	Stagnation
<i>cs</i>	Control surface	<i>v</i>	Virgin
<i>cw</i>	Cold wall	<i>w</i>	Wall
<i>e</i>	Outer edge of the boundary layer	<i>x, y</i>	Coordinates
<i>g</i>	Gas	∞	Freestream
<i>hw</i>	Hot wall		

Acronyms

ACE-SNL	Aerotherm Chemical Equilibrium - Sandia National Laboratory
ASCC	Ablation and Shape Change Code
CFD	Computational Fluid Dynamics
CFL	Courant-Friedrichs-Lewy
CMA	Charring Materials Ablation
COYOTE	Finite Element Computer Program for Non-linear Heat Conduction Problems
CVFEM	Control Volume Finite-Element Method
DPLR	Data Parallel Line Relaxation
FIAT	Fully Implicit Ablation and Thermal Analysis Program
IAPETUS	Interface pour l'Approximation des Proprietes a l'Equilibre Thermodynamique Utilisees dans les Simulations
LAURA	Langley Aerothermodynamic Upwind Relaxation Algorithm
LeMANS	“Le” Michigan Aerothermodynamics Navier-Stokes Solver
MOPAR	Modelling of Pyrolysis and Ablation Response
PICA	Phenolic Impregnated Carbon Ablator
SACCARA	Sandia Advanced Code for Compressible Aerothermodynamics Research and Analysis
SCMA	Super Charring Materials Ablation
SIRCA	Silicone Impregnated Reuseable Ceramic Ablator
SODDIT	Sandia One-Dimensional Direct and Inverse Thermal
TPS	Thermal Protection Systems

I. Introduction

The Thermal Protection System (TPS) of a re-entry vehicle is one of the key components of its design. The material used for the TPS can be classified into two main categories: ablative materials, as in the one used on Apollo missions, and non-ablative materials, such as the ceramic tiles used on the space shuttle. The former can also be divided into two sub-categories: charring (also know as pyrolyzing) and non-charring ablaters. The theory behind the use of ablaters is quite simple; the energy absorbed by the removal of material from the surface is not used to heat the TPS, thus keeping the vehicle at a reasonably “cold” temperature. In the case of charring ablaters, the ablative material is a resin which fills the pores of a carbon matrix. Although the matrix might ablate, it usually does not, thus preserving the original geometry of the aerodynamic surface during re-entry.

In order to correctly model the pyrolysis process, the gas generated from resin vaporization must be properly taken into account. Because this gas is expelled into the outer flow boundary layer, its effects are important in many aspects of re-entry modeling, such as carbon ablation, blowing effects in the boundary layer, chemical reactions with the surface, heat load, etc. The pressure of the gas within the ablator is also an important factor to take into account; if the pressure is too high, chunks of the ablator may “explode” without absorbing the expected amount of heat. This process, called spallation, may cause unwanted surface modifications and faster carbon ablation than anticipated, and thus may lead to the failure of the TPS.

As the first steps on an ongoing project on the modeling of heat transfer and ablation on hypersonic vehicles, such as re-entry capsules, the present study outlines different aspects of the importance of pyrolysis gas modeling. To do so, a thermal response code, named MOPAR, has been developed. First the governing equations describing the phenomenon are presented, and the code is validated against experimental data. Using realistic re-entry conditions, the code is also compared to the published results of other thermal

response codes. Using the latter test-case, the contribution of the kinetic energy is outlined, and conditions where this contribution may be relevant are discussed. For the same test-case, evidence of a non-Darcian flow regime is shown, and the use of Forchheimer number to categorize the flow type is proposed.

in order to fully assess the effects of material response on the flow field, and vice versa, the code is linked to the hypersonic viscous flow solver LeMANS. To validate the coupling method, a series of verifications are presented, showing excellent agreement to analytical solutions, empirical relations and other published data. Finally, in order to demonstrate the capability of the new coupled code, a simulation of a generic re-entry of the IRV-2 vehicle is presented, first using a surface ablator, and then a charring ablator.

II. MOPAR: Material response code

II.A. Governing equations and numerical scheme

The material response code presented here is based on a code developed at Sandia National Laboratory using a Control Volume Finite-Element Method (CVFEM).¹⁻⁵ The code can be used to model surface ablation with wall recession, as well as inner decomposition and pyrolysis gas behavior. The problem is described by the following four governing equations:

Mixture Energy Equation

$$\frac{d}{dt} \int_{cv} \rho E dV + \int_{cs} \phi \rho_g h_g v_g dA + \int_{cs} \dot{q}'' dA - \int_{cs} \rho h v_{cs} dA = 0 \quad (1)$$

Solid Phase Equation

$$\frac{d}{dt} \int_{cv} \rho_s dV - \int_{cs} \rho_s v_{cs} dA - \int_{cv} \dot{m}_s''' dV = 0 \quad (2)$$

Gas Phase Continuity Equation

$$\frac{d}{dt} \int_{cv} \phi \rho_g dV + \int_{cs} \phi \rho_g v_g dA - \int_{cs} \phi \rho_g v_{cs} dA - \int_{cv} \dot{m}_g''' dV = 0 \quad (3)$$

Momentum Equation

$$\frac{d}{dt} \int_{cv} \phi v_g \rho_g dV + \int_{cs} (\phi \rho_g v_g^2 + P) dA - \int_{cs} \phi v_g \rho_g v_{cs} dA - \int_{cs} \mu \frac{\partial v_g}{\partial x} dA = 0 \quad (4)$$

The first two equations are solved implicitly on an arbitrary contracting grid using Landau coordinates. Newton's method for non-linear systems is used to solve both equations sequentially. The third equation is straight forward, and does not need to be solved numerically. As for the last one, it is averaged to Forchheimer's Law, explicitly solved for v_g and directly integrated in the gas-phase continuity equation. The complete numerical treatment, as well as the numerical validations, are described in greater detail in Ref. 4. In addition to the improvement discussed in this paper, the present code also takes into account variable coordinate systems (cylindrical and spherical), as well as allowing ablation on both sides of the domain, using a new tri-diagonal solver.⁶

II.B. Model Validation

All the numerical validations presented in Ref. 4 are performed successfully on the code. This insures that MOPAR is coded properly and that the expected convergence behavior is respected. Since these results are exactly the same as those published in the reference, and since they serve no purpose in the context of this paper, they are omitted here. Two other validations are however presented: they demonstrate the validity of the code as a model.

Code-to-Code comparison

The first validation compares the present code to the one developed at Sandia National Labs Ref. 4, which was extensively compared to the old CMA code⁷ as well as Sandia's SODDIT.⁸ The simulation is performed

using solid and gas properties given in Ref. 4, as are the re-entry conditions used on the ablative surface, shown in Fig. 1. Hot wall and blowing corrections are applied to the incident aeroheating flux; thermal-radiation cooling is also used. The calculations are performed on a 50 element logarithmic grid, with a 1.01 progression, over a 1.27 cm domain, using time steps of 0.2 s. The thermochemical table is generated using ACE-SNL.⁹

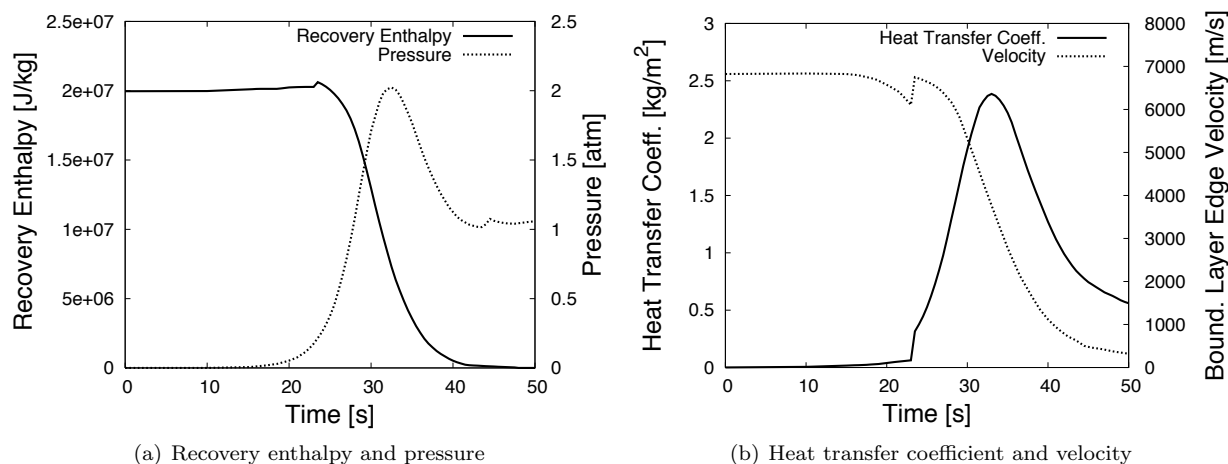


Figure 1. Re-entry conditions for the first validation (the discontinuity on each curve is caused by the transition to turbulent flow)

Figure 2 presents the comparison of this validation for surface temperature and surface recession. As expected, the surface temperature from both simulations agree quite well. The discrepancy that occurs at the end of the simulation is due to the fact that the precise re-entry conditions could not be obtained. As for the surface recession, the discrepancy is solely due to the fact that different thermochemical tables are used. Because of this, the general agreement of both curves is considered satisfactory.

Comparison to experimental results

The second validation presented here compares the code to two experiments.¹⁰ For these test-cases, a 1.27 cm carbon-phenolic material is exposed to an air arc-jet flow for which the parameters are listed in Table 1.

Table 1. Test conditions for the heat transfer blowing correction verification

Test case	H_{st} [J/kg]	q_{st} [W/m ²]	p_{st} [Pa]	Δt [s]
1	11.60×10^6	1.44×10^6	0.07	60
2	26.65×10^6	7.05×10^6	0.32	35.0

The calculations are performed on a 150 element logarithmic grid, with a 1.01 progression, using a constant time marching of 0.1 s. A blowing correction as well as a hot wall correction are applied to the incident heat flux. Solid and gas properties used in this simulation are the same as those given in Ref. 10, except for the pyrolysis gas, which uses data from Ref. 11, and porous parameters ϕ and K , which are taken from Ref. 4. For the ablation model, the generic thermochemical carbon-phenolic ablation table obtained from Ref. 4 is used. Since the code is designed to have the heat transfer coefficient as an input, and not the heat flux, the specified conditions cause problems. The equation that links the heat flux to the heat transfer coefficient is:

$$C_e = \rho_e u_e St = \frac{q}{H_r - h_w}$$

Therefore, to apply the correct boundary conditions to the surface, the recovery enthalpy and the enthalpy at the wall must be known. The first of these quantities can be approximated to the stagnation enthalpy, but the other is only known when the ablation model (i.e. thermochemical table) is evaluated. In order to

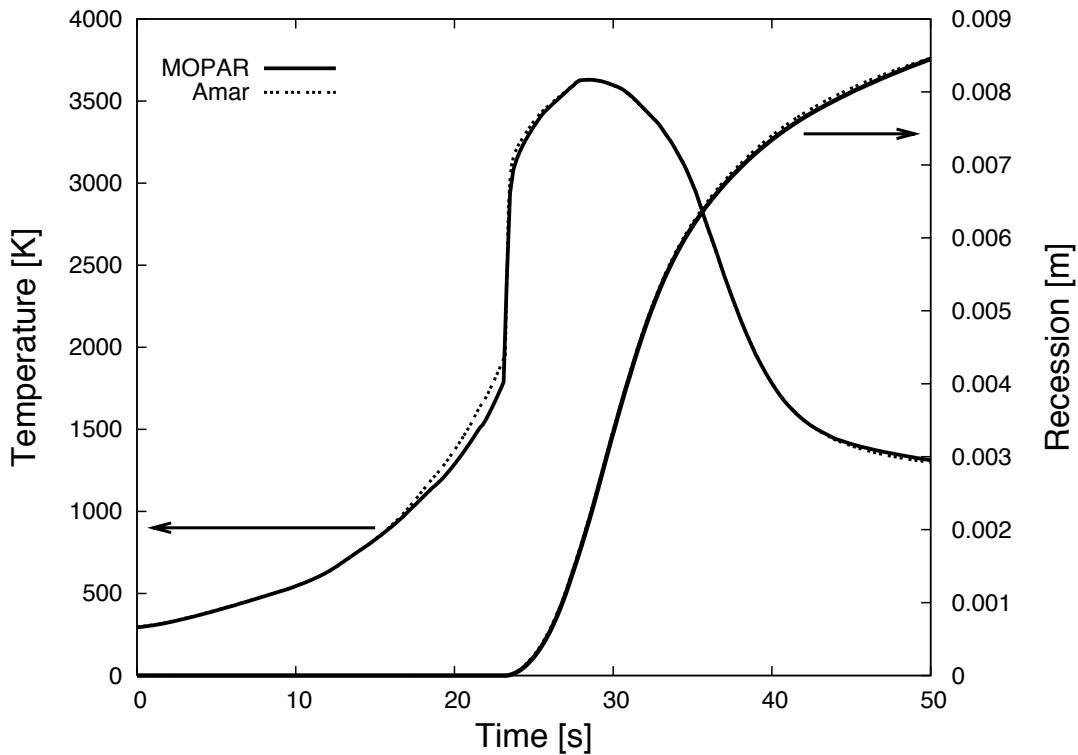


Figure 2. Comparison of surface temperature and surface recession between CMA and present work for re-entry validation

correct this problem, the code is initially run with a C_e calculated using a wall enthalpy of zero. After this initial run, the computed wall enthalpy is used to calculate a new C_e , which is used for another run. The code iterates over the trajectory until a converged value for the wall enthalpy is obtained.

The graphs of Fig. 3 show the comparisons for surface and back temperature, surface recession and pyrolysis front recession. For both test-cases, the computer prediction is well within the acceptable ranges of the experimental results. The discrepancies can be attributed to the generic carbon-phenolic thermochemical table, as well as a slightly different pyrolysis gas.

Because the exact method used to experimentally measure the pyrolysis front is not described, a value of 50% of resin has been chosen as the approximation of the char/virgin interface. This choice is justified by the fact that the pyrolysis front is quite steep, as illustrated in Fig. 4, and that Arrhenius-type relations are used to describe the chemical decomposition. As mentioned in Ref. 10, the discrepancy between the simulation and the experimental results, as far as the recession rates are concerned, is caused by the fact that the cool down period is not taken into account. This cool down period is simulated by simply setting the heating boundary conditions to zero, and only using re-radiation as the cooling mechanism. As in Ref. 10, it was observed that in both cases, the pyrolysis front kept on going, reaching the back surface at approximately 75 seconds for the first test-case, and 42 seconds for the second one. In reality, the test pieces were quenched by argon right after the arc-jet exposure, in an attempt to stop the chemistry as soon as possible: since no exact description of the process is available, it is not possible to produce an accurate cool down model.

The discrepancy on the surface ablation front is, obviously, not caused by the cool-down since ablation immediately stops after exposure, and the simulation over predicts the distance. This difference can be attributed to two reasons: first, the empirical thermochemical tables used are not generated for the specific carbon-phenolic material of the experiment (Narmco 4028). Also, thermal expansion of the test-pieces was

observed, and is not included in the present model. Depending on the type of material, as well as the fiber's orientation, this process might not necessarily be reversible, thus causing variations in the thickness that could potentially cancel the effect of ablation front measurements.

II.C. Kinetic Energy

In order for the governing equations to be rigorous, the kinetic energy must be included in the Mixture Energy Equation, Eq. (1). Kinetic energy is added in the time-dependent energy content term (first term), the gas flux term (second term) and the grid convection term (fourth term). The contributions in the control volume are:

Energy Content Term

$$\tilde{E}_K = \frac{d}{dt} \int_{cv} \rho \frac{v_g^2}{2} dV$$

Gas Flux Term

$$\dot{G}_K = \int_{cs} \phi \rho_g \frac{v_g^2}{2} v_g dA$$

Grid Convection Term

$$\dot{E}_K = - \int_{cs} \rho \frac{v_g^2}{2} v_{cs} dA$$

In the re-entry test case described in the previous section, the addition of these terms has little to no effect on the final results, thus validating their omission in most Thermal Response codes (CMA,⁷ Sandia National Labs,² FIAT;¹² however SCMA,¹³ in its latest version, uses these contributions). As seen in Fig. 5, the difference between the kinetic terms and the other terms is several orders of magnitude. It is to be noted that depending on the charring material used, these effects may start to appear. A material with a very high rate of decomposition, as well as high porosity, may lead to higher gas velocity. With a simple correlation using the velocity shown in Fig. 6, it is possible to estimate that a gas velocity of the order of 100 m/s (i.e., an increase of one order of magnitude) would allow the contributions shown in Fig. 5(b) to register in Fig. 5(a).

II.D. Forchheimer's Law

In other works, either Darcy's law² or Forchheimer's Law^{7,13} is used to calculate the velocity of the gas within the ablator. The choice of the law is somewhat unclear as it is correlated to the Reynolds number. As pointed out in Ref. 14, there is enormous disagreement on the conditions where a flow is not described by Darcy's equation. Usually, the Reynolds number based on pore length is used to describe this condition. However, since this number describes microscopic effects, it is inappropriate to validate the use of a law describing macroscopic effects; all attempts to do so are based on different interpretations as to what should be the characteristic length used. To better address this problem, a new formulation of Forchheimer's Law was recently proposed.¹⁵ In Cartesian geometry, this equation is:

$$\frac{\partial P}{\partial x} = - \frac{\mu}{K} v_g' (1 + \text{Fo}) \quad (5)$$

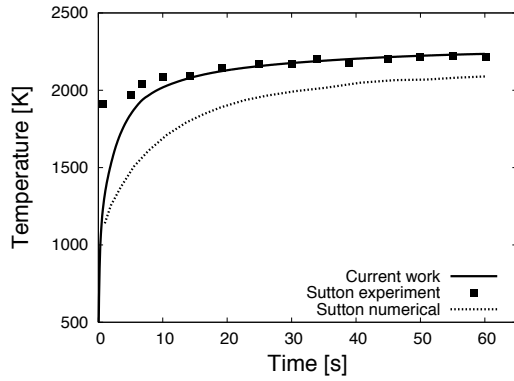
where Fo, the Forchheimer number, is given by:

$$\text{Fo} = \frac{\beta K \rho v_g'}{\mu}$$

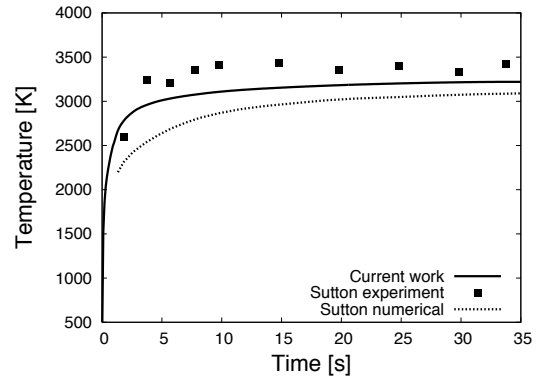
This number indicates when microscopic effects (pore-size) are perceivable at a macroscopic (geometry size) level. In this formulation, it is easy to see that when $\text{Fo} \ll 1$, the equation simply reduces to Darcy's law. Therefore, it is more logical to use the Forchheimer number to predict non-Darcian flow, and thus more rigorous to use Forchheimer's law in the code.

The law can be derived from the momentum equation, using averaging methods:¹⁶

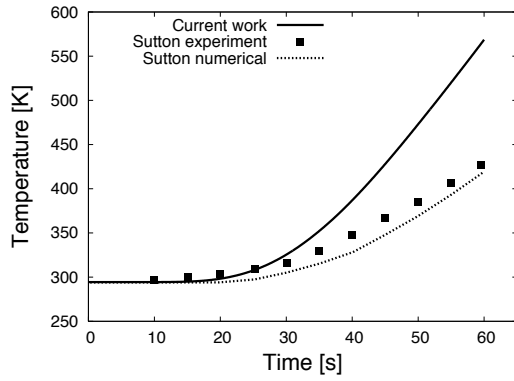
$$\rho \left(\frac{\partial v_g}{\partial t} + v_g \frac{\partial v_g}{\partial x} \right) + \frac{\partial P}{\partial x} = \mu \frac{\partial^2 v_g}{\partial x^2}$$



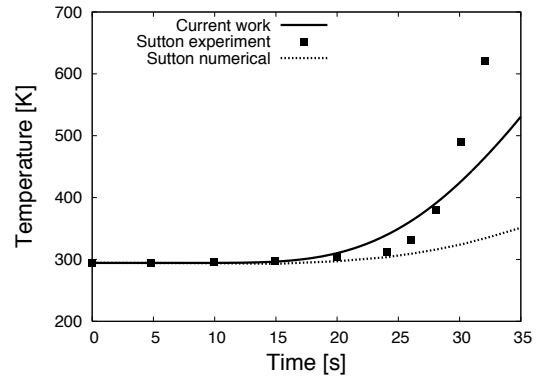
(a) Surface temperature for test-case 1



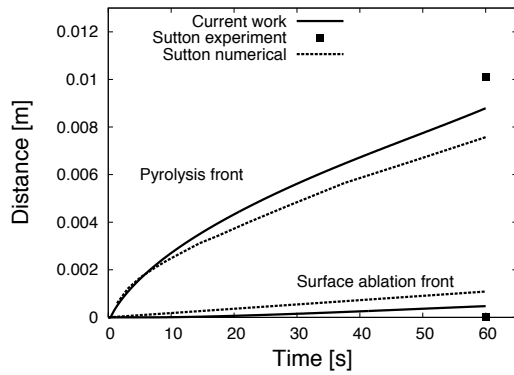
(b) Surface temperature for test-case 2



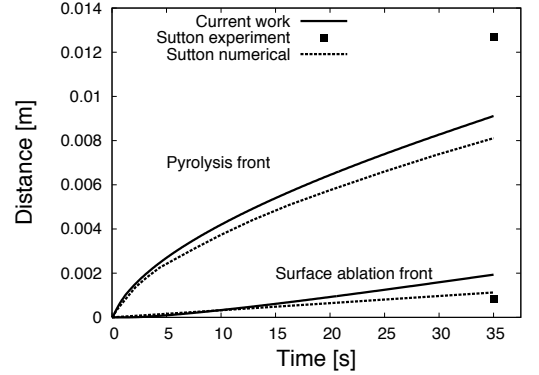
(c) Back face temperature for test-case 1



(d) Back face temperature for test-case 2



(e) Surface ablation and pyrolysis front for test-case 1



(f) Surface ablation and pyrolysis front for test-case 2

Figure 3. Comparisons of the present code to experimental results

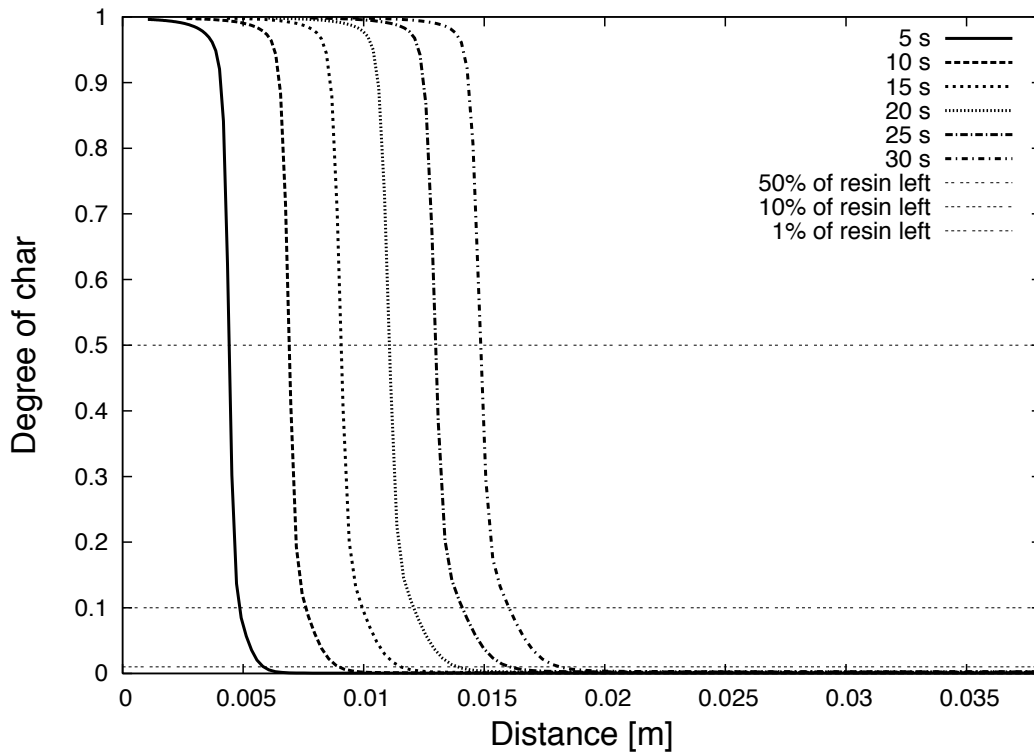


Figure 4. Evolution of the pyrolysis (char) front for the second validation. The degree of char is obtain using the ratio of ablated resin density to initial resin density $(\rho_v - \rho_s)/(\rho_v - \rho_c)$

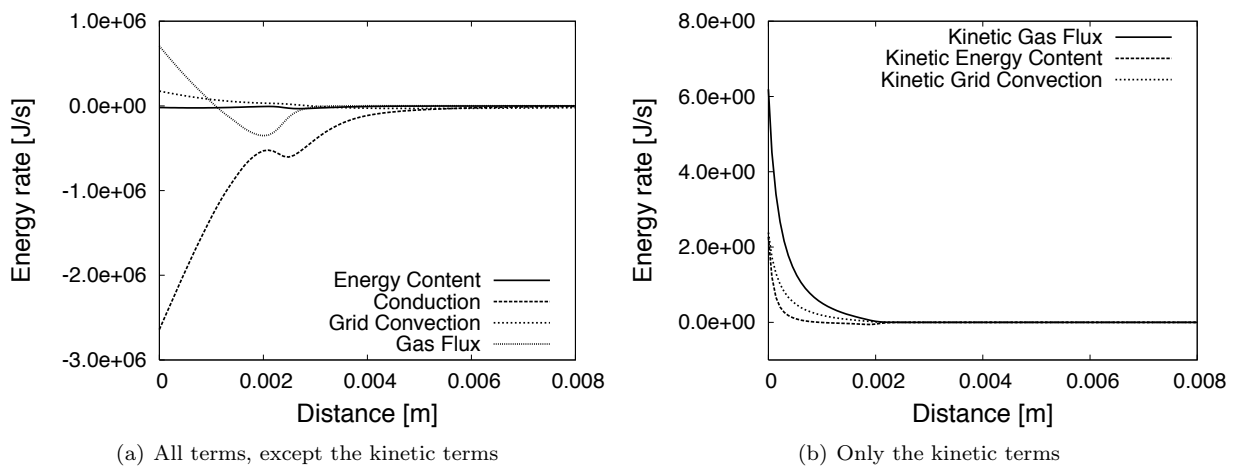
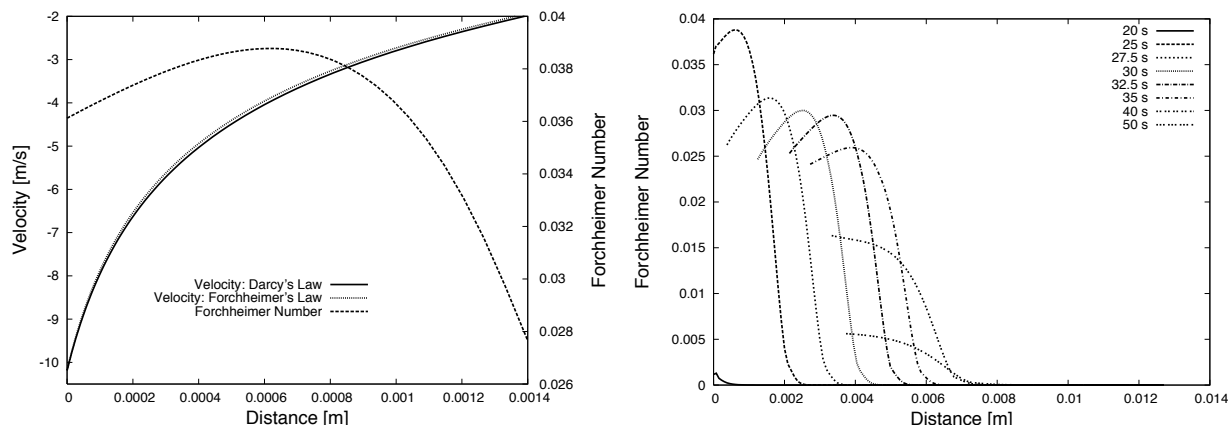


Figure 5. Energy rates of each contributing term of the Mixture Energy Equation, taken at $t = 25$ seconds of the trajectory

One can also obtain the same results by simply dimensionalizing the equation of momentum, replacing the spatial derivative by the inverse of the square root of the permeability K and the velocity by the superficial velocity v'_g . As for the parameter β , it may be obtained experimentally if the pore configuration of the material is unknown.

Figure 6(a) shows the difference in gas velocity for both methods, for the case of the re-entry simulation presented earlier, at $t = 25$ seconds. Figure 6(b) shows the Forchheimer number for different times during the whole simulation. As seen, the value of Fo is of the order of 0.01; by inserting this value in Eq. (5), it can be seen that the effects, although small, are non-negligible.



(a) Comparison of the internal gas velocity calculated using Darcy's Law and Forchheimer's Law ($\beta = 3.0/\sqrt{K}$) during re-entry, at $t = 25$ seconds, using a 150 element grid of 1.05 logarithmic progression

(b) Forchheimer number at various times during the re-entry simulation

Figure 6. Forchheimer number for the generic re-entry simulation of Fig. 1

Although many studies have been performed^{17–19} on the behavior of pyrolysis gas, none account for the possibility of β being a significant factor. A simple parametric study allows one to see that even though there is little to no effect on the temperature of the material, other quantities such as velocity, density and, obviously, pressure are greatly affected. The graphs of Fig. 7 show the behavior of the pyrolysis gas at the 30 s re-entry point of the generic trajectory used in the previous section. It can clearly be seen that as soon as Forchheimer's number becomes greater than 1 ($\beta_K = 30$), notable effects appear. Given that spallation has been observed¹⁰ in many materials considered for re-entry systems, it is therefore important to take these effects into account. It is clear that such a high pressure zone as the one that appears near the wall-flow boundary will cause spallation.

The main obstacle in using Forchheimer's Law remains the knowledge of parameter β . Ergun²⁰ linked that parameter to $1/\sqrt{K}$. It is interesting to note that with that definition, the Forchheimer number becomes:

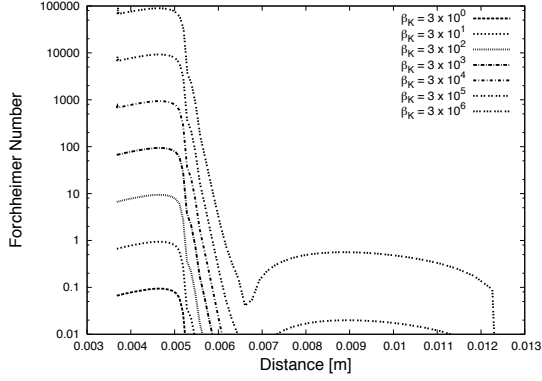
$$Fo = \beta_K \frac{\sqrt{K} \rho |v'_g|}{\mu}$$

which is basically Reynolds number defined with a characteristic length of \sqrt{K} and multiplied by the experimentally defined parameter β_K . For carbon-phenolic, the latter has been evaluated as 1.222.^{13,21}

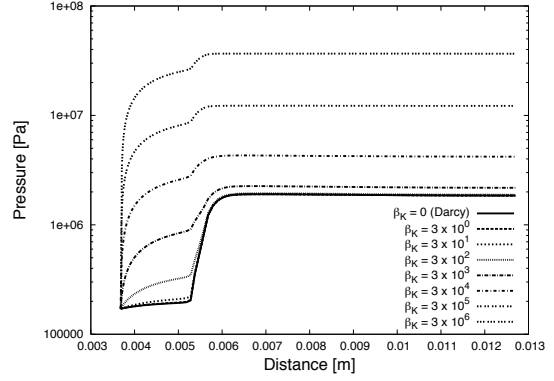
In order to obtain values for β or β_K , the experimental setup and method of Ref. 14 could be used. With this methodology, already published experimental data^{22–24} could easily be employed to calculate β for two frequently used charring ablators, PICA and SIRCA. However, other experimental values, notably the length of the test pieces and pressure at both ends, would have to be known. It is also important to point out that the deviation from Darcy's Law presented in Ref. 22, the sometimes called "Klinkenberg model", is not in any way related to the additional effects contained in Forchheimer's Law. While the latter takes into account high velocity effects, the former models the slip-flow hypothesis of the gas within porous media. The relation used to calculate permeability is

$$K = K_0 (1 + b/P)$$

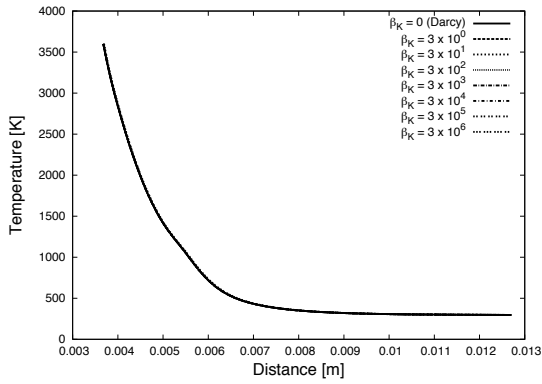
In this equation, permeability coefficient b is a function of the gas composition, unlike K_0 , the permeability



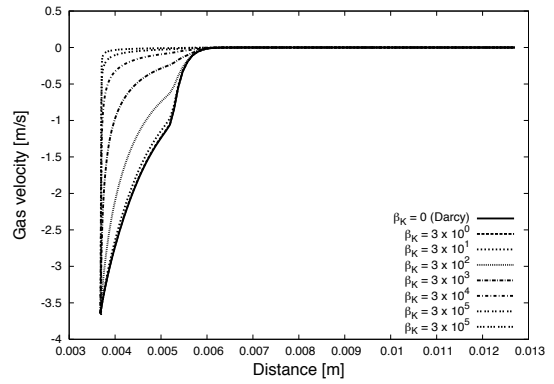
(a) Forchheimer number



(b) Pressure



(c) Temperature



(d) Velocity

Figure 7. Influence of inertial parameter β on the internal gas behavior: β varies from 0 to 3×10^6

in the no-slip regime, which is only material dependent. It is also to be noted that both these parameters are also found experimentally.

III. Coupling with a flow solver

III.A. The hypersonic CFD code LeMANS

In order to more accurately investigate the effects of the flow field on the material, it is necessary to couple the material response to a Navier-Stokes solver. LeMANS is a finite volume Navier-Stokes solver currently being developed at The University of Michigan.^{25–28} The code assumes that the rotational and translational energy modes of all species can be described by a single temperature T , and that the vibrational energy mode of all species and the electronic energy can be described by a single temperature T_v . The latter is computed using the species vibrational energy, modeled as a harmonic oscillator. The viscous stresses are modeled assuming a Newtonian fluid, using Stokes hypothesis, and the species mass diffusion fluxes are modeled using a modified version of Fick’s law. Mixture transport properties are calculated using one of two models; the first uses Wilkes semi-empirical mixing rule with species viscosities calculated using Blottner’s model and species thermal conductivities determined using Eucken’s relation. The other uses Gupta’s mixing rule with species viscosities and thermal conductivities calculated using non-coulombic/coulombic collision cross section data. As for the heat fluxes, they are modeled according to Fourier’s law for both temperatures. Finally, the source terms of the species conservation equation are modeled using a standard finite-rate

chemistry model for reacting air in conjunction with Park’s two-temperature model to account for thermal nonequilibrium effects on the reaction rates.

Numerically, the code has the capability to handle meshes containing any mix of hexahedra, tetrahedra, prisms and pyramids in 3D or triangles and quadrilaterals in 2D. Numerical fluxes between the cells are discretized using a modified Steger-Warming Flux Vector Splitting which has low dissipation and is appropriate to calculate boundary layers. A point or line implicit method is used to perform the time integration, and the calculation can be performed efficiently over a large number of parallel processors. The code has been extensively validated against experimental data, and has also been compared to similar codes such as NASA Ames’ DPLR²⁹ and NASA Langley’s LAURA.³⁰

Blowing boundary conditions

Because of the coupling, ablation is added to the CFD code; therefore, a modification to the surface boundary condition is necessary. In order to implement the blowing boundary condition, the first cell near the blowing wall is used as a control volume.³¹ The physical values that need to be imposed at the wall are the temperature T_w , the blowing mass flow rate $\dot{m}_w = \rho_w v_w$ and the species mass fraction Y_{wi} . The conservation of momentum is applied using both the perpendicular face or the cell, assuming that the flow is only perpendicular to the surface:

$$p_\eta = p_{nc} + \rho_{nc} v_{nc}^2 = p_w(\rho_w, T_w) + \rho_w v_w^2$$

Using the perfect gas relation at the wall, the equation can be rearranged to obtain the primitive variables:

$$\rho_w = \frac{p_\eta + \sqrt{p_\eta^2 - 4RT_w \dot{m}_w^2}}{2RT_w}$$

$$v_w = \frac{2RT_w \dot{m}_w}{p_\eta + \sqrt{p_\eta^2 - 4RT_w \dot{m}_w^2}}$$

$$p_w = \frac{p_\eta + \sqrt{p_\eta^2 - 4RT_w \dot{m}_w^2}}{2}$$

Once these values are computed, the conservative quantities in the ghost cells of the boundary are set such that the flux across the wall is the required blowing flux. This blowing boundary condition has been tested over a wide range of blowing rates, assuring the robustness of the implementation. Following the methodology for the verification and validations of NASA Ames’ DPLR code³² and NASA Langley’s LAURA code,³¹ the blowing boundary of LeMANS is also verified and validated.

Blasius analytical solution

As a first verification, a simulation of the Blasius analytical approximation for a flow over a flat plate with blowing and suction is performed. In this approximation, the analytical solution is obtain by solving

$$f' + f f'' = 0$$

where $f'(\eta) = 2 \frac{u}{u_\infty}$, with $\eta = \frac{1}{2} \sqrt{\text{Re}_x} \frac{y}{x}$ and $\text{Re}_x = \frac{u_\infty x}{\nu}$. The mass flow rate is imposed directly in LeMANS, using the following relation:

$$\dot{m}_w = \rho_\infty u_\infty \frac{-f(0)}{2\sqrt{\text{Re}_x}}$$

In order to insure that no perturbation arises from the inlet and outlet boundary conditions and that the flow is allowed to fully develop after and before the 1 m flat plate, a large computation domain of 10 m in all directions is used. The free stream conditions are set to normal pressure and temperature, at a velocity of Mach 0.3, which is the limit of the incompressible flow assumption, and therefore, the limit of the Blasius solution. Figure 8 shows the comparison between the simulation and the analytical solution tabulated by Ref. 33 for the regular Blasius profile ($f(0) = 0$), blowing ($f(0) = -0.4, -0.8$) and suction ($f(0) = 1.2, 5.0$). Even though there are minor discrepancies between both solutions, the general trends of the curves show good agreement, and are sufficiently close to confirm the correct implementation.

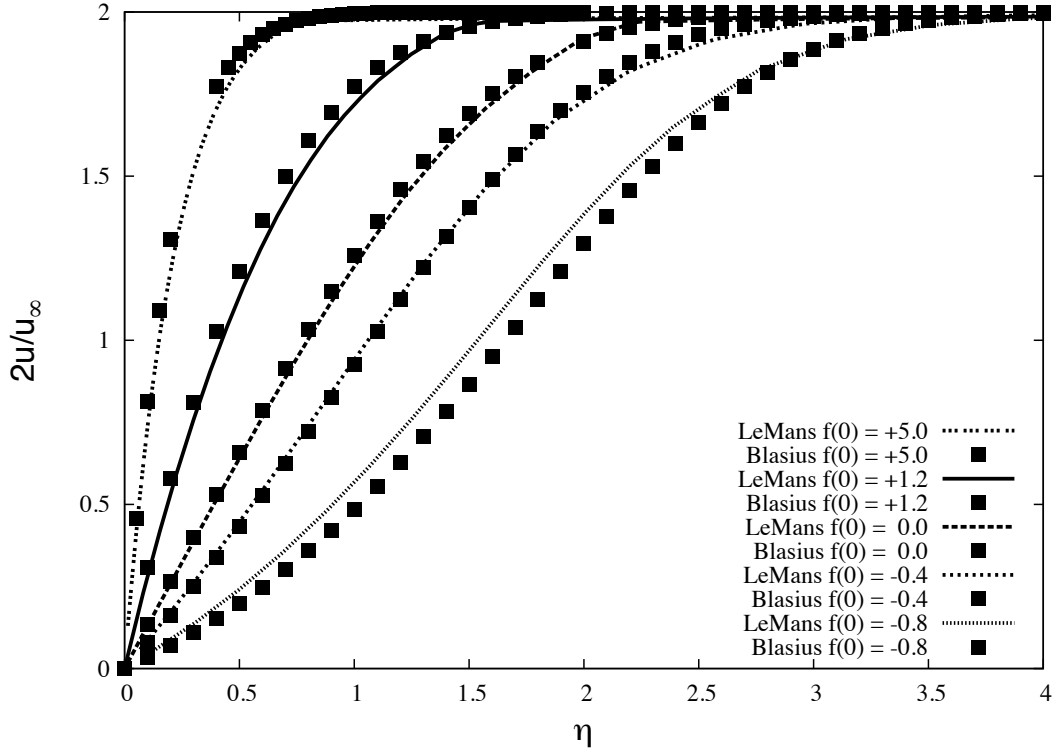


Figure 8. Comparison between analytical and numerical results for the Blasius blowing boundary conditions

Crawford and Kay's blowing correction on heat transfer

To take into account the heat flux reduction caused by the blowing in the boundary layer, Crawford and Kays³⁴ established a simple relation:

$$\Omega_{bw} = \frac{q}{q_0} = \frac{\ln(B' + 1)}{B'}$$

which was later extended to include the fitting parameter λ :

$$\Omega_{bw} = \frac{\ln(2\lambda B' + 1)}{2\lambda B'}$$

where

$$B' = \frac{\dot{m}_w}{\rho_e u_e St}$$

is the non-dimensionalized blowing rate, calculated using the Stanton Number

$$St = \frac{q}{\rho_e u_e (H_r - h_w)}$$

The parameter λ usually takes the value of 0.4 for laminar flow, and 0.5 for turbulent; however, it has recently been established that these values are not accurate in multiple regimes.³² Nevertheless, the equation can be used to validate the general trends of the heat flux. In order to do so, four different Couette flow test-cases are run; the detailed conditions of each simulation are presented in Table 2. As can be seen in Figs. 9 and 10, the simulation results obtained with LeMANS agree with the empirical relation for all cases. However,

it is to be noted that none of the simulations have a close fit to the $\alpha = 0.4$ analytical solution: 0.5 and 0.6 are a better match for subsonic flow, and 0.3 for supersonic. It is also interesting to note the difference in the general trend of the curves for the subsonic and supersonic regimes.

Table 2. Test conditions for the heat transfer blowing correction verification

Test case	u_∞ [m/s]	T_∞ [K]	ρ_∞ [kg/m ³]	T_w [K]	\dot{m}_w [kg/m ² /s]
1	102.087	1490.75	1.183925154	298.15	0.005
2	102.087	1490.75	1.183925154	298.15	0.05
3	1020.87	1490.75	0.1183925154	298.15	0.005
4	1020.87	1490.75	0.1183925154	298.15	0.05

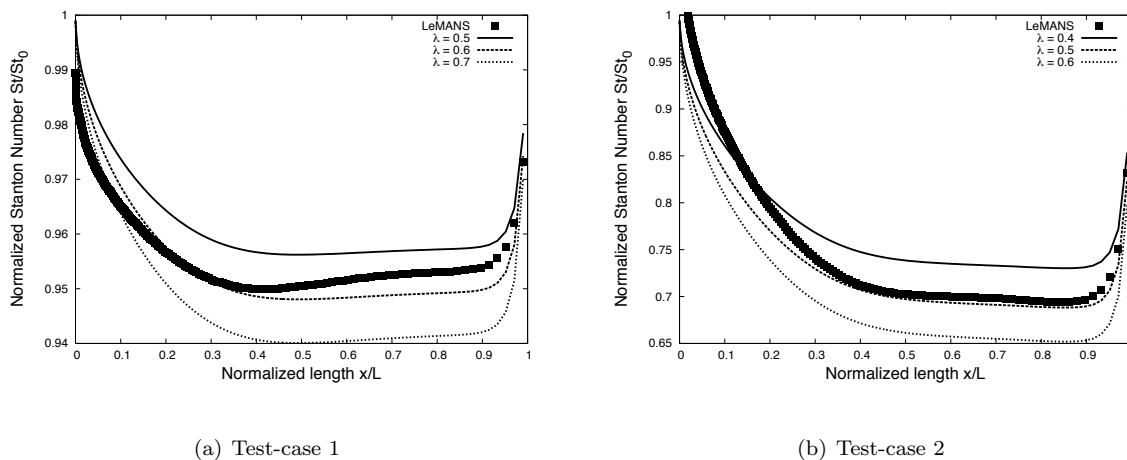


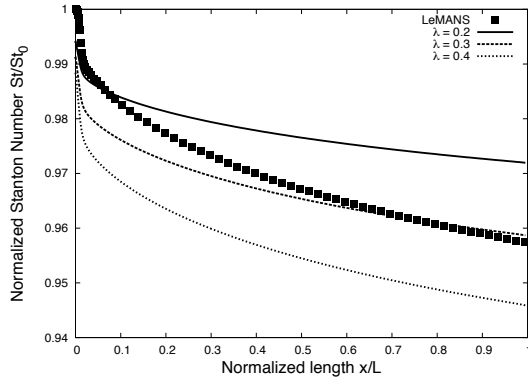
Figure 9. Subsonic (Mach 0.13) laminar blowing correction for test-cases 1 and 2 of Table 2

III.B. Thermal response coupling

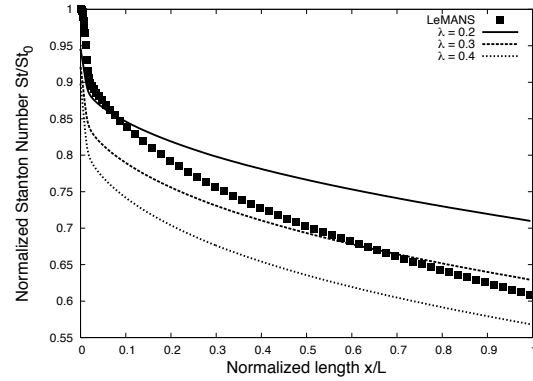
Because re-entry simulations are being performed by computing steady-state solutions at multiple points of a discretized trajectory, it is possible to directly integrate the thermal response code in the boundary condition subroutines of LeMANS, and thus take advantage of the implicit nature of the code as well as the aggressive CFL ramping. The method used is similar to the one described in Ref. 35, and is illustrated in Fig. 11. Since MOPAR is 1-D, normal solution lines within the wall are traced at each boundary cell, and are computed sequentially. Because there is no need to compute the material response at every flow field iteration, MOPAR is called at a pre-fixed number of iterations. To optimize the coupling method, a sensitivity study will be made in order for the code to automatically decide when thermal response coupling is necessary. It is to be noted that since the flow field chemistry of LeMANS has yet to be implemented, the mass fractions, even if they are computed, are not used for the surface composition. The code used for that calculation is IAPETUS, and was originally developed for the computation of thermal properties in high temperature flows.³⁶⁻³⁹ In order to speed-up convergence, the convective heat flux used in MOPAR is adjusted using a hot-wall correction:⁴⁰

$$q_{hw} = q_{cw} \Omega_{hw} = q_{cw} \left[\frac{\rho(T_{hw}, p_w) \mu(T_{hw})}{\rho(T_{cw}, p_w) \mu(T_{cw})} \right]^{0.1}$$

The use of this correction speeds up the convergence of the wall temperature and ablation rates, therefore not affecting the convergence of LeMANS. Figure 12 shows a comparison between the convergence history



(a) Test-case 3



(b) Test-case 4

Figure 10. Supersonic (Mach 1.3) laminar blowing correction for test-cases 3 and 4 of Table 2

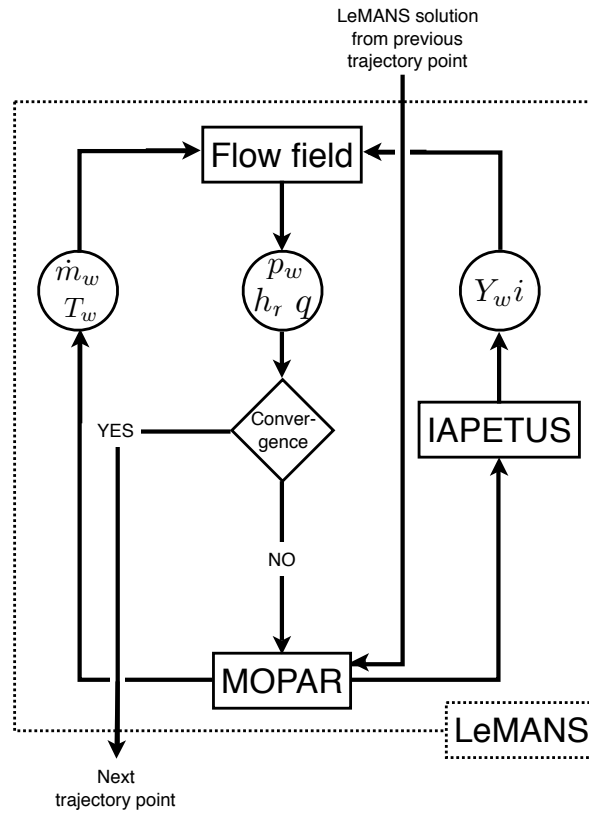


Figure 11. Coupling procedure for the integration of MOPAR in LeMANS

of a simulation of the IRV-2 vehicle, at re-entry point 16 of Table 3, using a re-radiating wall temperature boundary condition and the coupled method. The simulation uses ramping CFL number, with initial conditions set to the converged solution at the previous trajectory point, using their respective wall temperature boundary. For this coupled case MOPAR is called every 100 iterations, which translates as small spikes on the convergence history. As seen in the graph, the two curves are very similar and follow the same trend; therefore, even if wall-clock time is obviously affected, the convergence remains the same.

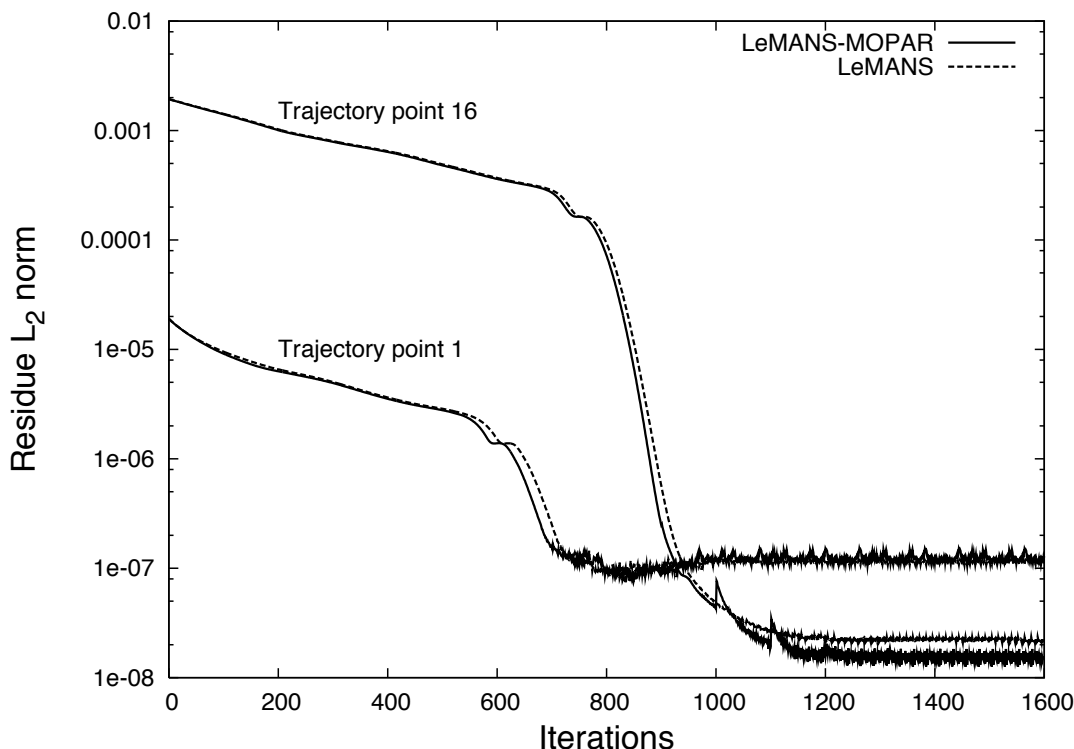


Figure 12. Convergence to steady state for the IRV-2 vehicle, at trajectory points 1 and 16: comparison between the regular solution and the coupled method

IRV-2 test-case

In order to validate the coupling between MOPAR and LeMANS, the well documented^{31,35} re-entry simulation of an IRV-2 vehicle is performed. The freestream conditions used in the discretized trajectory are presented in Table 3, and the material properties are set to generic non-charring carbon, using the properties given by Ref. 4. The ablation rates are interpolated from thermochemical tables generated by ACE-SNL⁹ for carbon in air. Re-radiation is also included at the boundary. Examples of the coupled results are presented in Fig. 14, and the temperature at the stagnation point for the whole re-entry trajectory is shown in Fig. 13. The results are in the same range as those published in the literature; the discrepancy is due to the lack of proper chemistry model and moving mesh in the flow field. It is to be noted that the overvaluation in the first part of the trajectory, as well as the smoothness of the curve, is due to the fact that the whole material response surface history is plotted, as opposed to only the value at the discretized trajectory points. In general, the coupled algorithm proves to be fast and robust for all the trajectory points.

Finally, in order to demonstrate the capabilities of the coupling method, the same trajectory is run using carbon-phenolic material as the ablator. The solid properties used for this calculation are the same as the first validation. Because MOPAR is called several times during the simulation, the wall enthalpy iterative

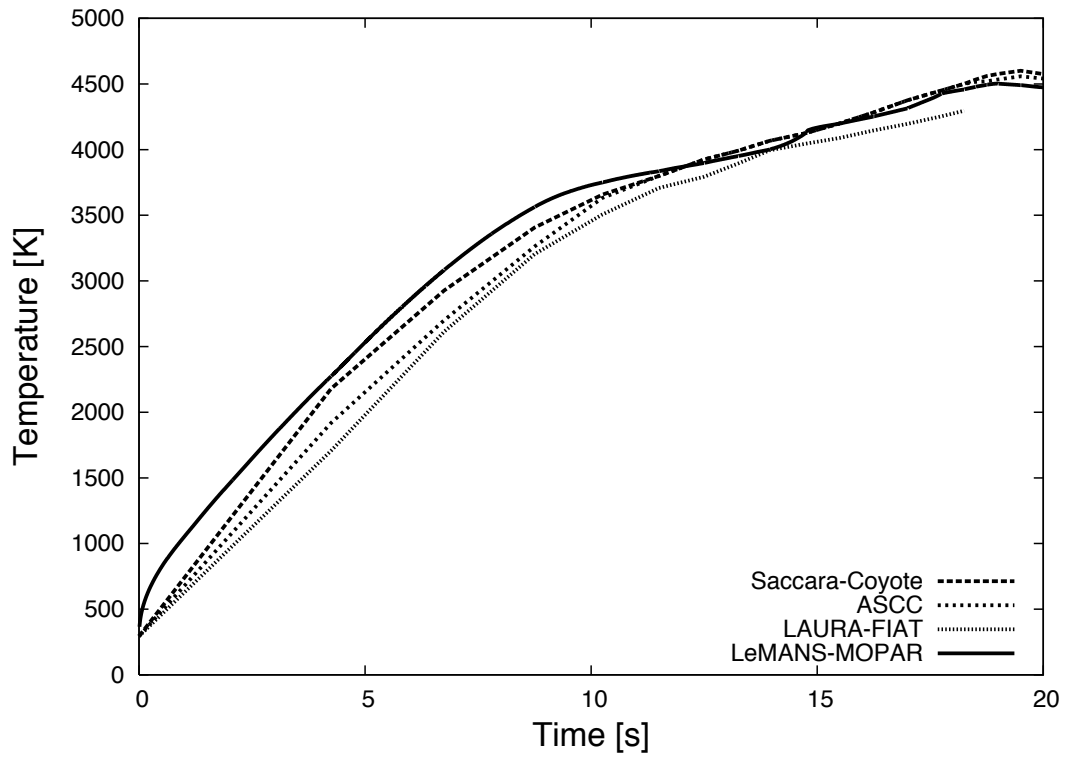


Figure 13. Temperature at the stagnation point of the IRV-2 re-entry vehicle at the trajectory points of Table 3: comparison with numerical results of Ref. 35 and Ref. 31

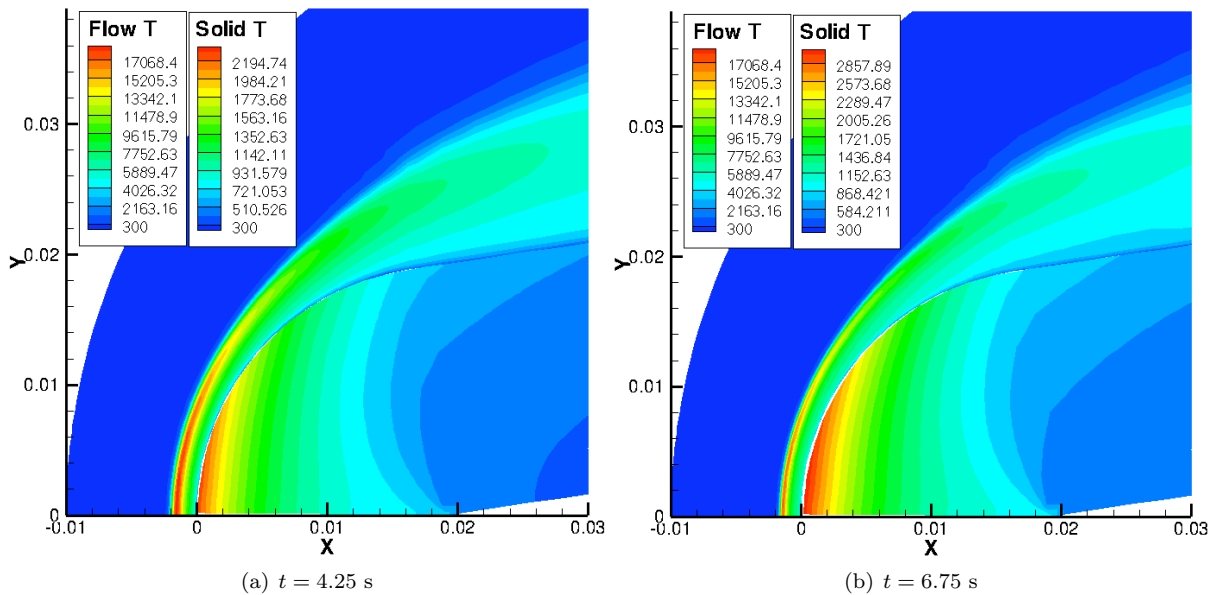


Figure 14. Temperature distribution of the flow field and in the solid wall of the IRV-2 re-entry vehicle at trajectory points 2 and 3 of Table 3

Table 3. Freestream conditions for the re-entry trajectory of the IRV-2 vehicle (from Ref. 35)

Trajectory point	Time [s]	Velocity [m/s]	Temperature [K]	Density [kg/m ³]
1	0.00	6780.6	227.81	1.2505×10^{-4}
2	4.25	6788.3	258.02	5.0454×10^{-4}
3	6.75	6785.2	270.65	1.1344×10^{-3}
4	8.75	6773.0	261.40	2.2593×10^{-3}
5	10.25	6752.4	250.35	3.9957×10^{-3}
6	11.50	6722.0	241.50	6.4268×10^{-3}
7	12.50	6684.3	234.30	9.5832×10^{-3}
8	13.25	6644.9	228.76	1.3145×10^{-2}
9	13.95	6596.7	226.91	1.7313×10^{-2}
10	14.75	6527.1	224.73	2.4310×10^{-2}
11	15.50	6428.3	222.35	3.5348×10^{-2}
12	16.25	6286.6	219.47	5.5888×10^{-2}
13	17.00	6091.7	216.65	9.1741×10^{-2}
14	17.75	5836.4	216.65	1.5635×10^{-1}
15	18.25	5631.8	216.65	2.2786×10^{-1}
16	18.50	5519.6	216.65	2.7946×10^{-1}
17	18.75	5401.2	216.65	3.3743×10^{-1}
18	19.00	5277.1	221.31	3.9840×10^{-1}
19	19.50	5014.3	236.86	5.3196×10^{-1}
20	20.00	4736.5	252.11	6.9366×10^{-1}

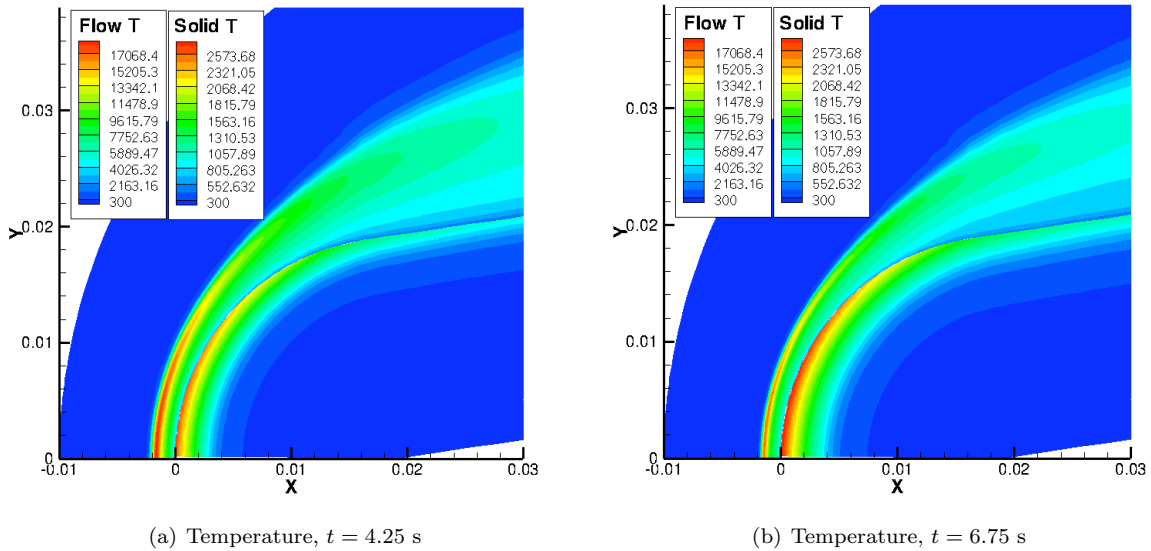


Figure 15. Temperature distribution of the flow field and in the solid wall of the IRV-2 re-entry vehicle at trajectory points 2 and 3 of Table 3 ,with carbon-phenolic as material

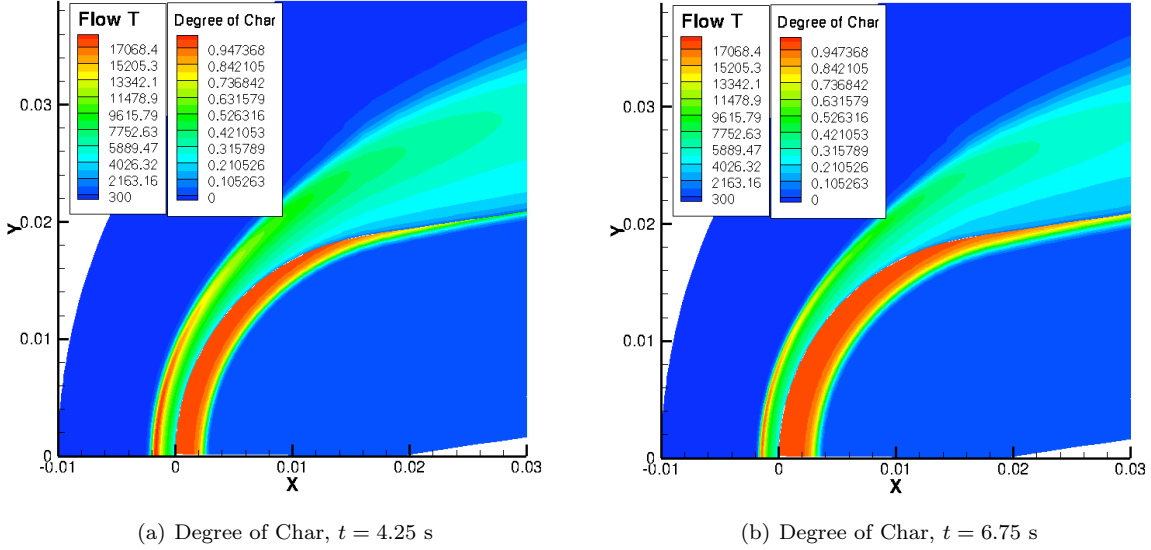


Figure 16. Temperature distribution of the flow field and degree of char of the solid wall of the IRV-2 re-entry vehicle at trajectory points 2 and 3 of Table 3 ,with carbon-phenolic as material

process described in II.B is performed over the whole calculation, and not at each MOPAR call. Figures 15 and 16 shows the results for the temperature and the degree of char for trajectory points 2 and 3 of Table 3. It is interesting to compare Figs. 15 and 14: it can be clearly seen that the carbon-phenolic is able to sustain the heat without ablating. Also, the absorbed heat does not penetrate into the wall as much as for regular ablating carbon; this translates into a cooler, undisturbed, inner temperature.

IV. Conclusion

As part of a continuing project to improve heat and ablation rate modeling on re-entry vehicles, a one-dimensional material response implicit solver that includes pyrolysis and surface ablation has been presented. The new developments can now show a more precise contribution of the pyrolysis gas to the behavior of the Thermal Protection System (TPS). More specifically, the usage of the Forchheimer number as an indicator of non-Darcian flow behavior has been highlighted. The code has been validated using experimental data, and code-to-code comparison. Finally, the evidence of non-Darcian behavior has been shown using a simple re-entry trajectory with a generic carbon-phenolic ablator.

Most importantly, the material response code was iteratively coupled to the hypersonic CFD code LeMANS. Verifications of the blowing boundary condition were presented, using two semi-analytical cases. The first, based on the Blasius solution of the boundary layer problem, shows excellent agreement with the simulation results. The second, based on Crawford and Kays' blowing correction, also produces good results; the previously discussed problem with the fitting parameter λ was also observed. As a first step towards the validation of the coupling algorithm between the flow solver LeMANS and the material response code MOPAR, the simulation of the re-entry trajectory of an IRV-2 vehicle was presented. The numerical results are within the expected range, and the coupling method used shows robustness and efficiency during the simulation.

This paper presents the first steps towards the development of an accurate model for flow-solid thermal interactions. Even if in its current state, it shows excellent results, more features should be added. First, the outer flow chemistry model needs to be modified to add the possible chemical reactions of the pyrolyzing and ablating gases with the atmosphere. Also, an interactive moving grid subroutine needs to be added to the coupling mechanism to account for the wall recession in the flow field calculation. Last, but certainly not least, an ablation model that accounts for surface chemistry without relying on thermochemical tables^{41,42} should be added to increase the accuracy of the overall model. As for the modifications of the thermal response code, a spallation model⁴³ can be added to account for high pressure rises.

Acknowledgments

The authors would like to thank the *Government of Québec* which, through the *Fonds de recherche sur la nature et les technologies*, provides a fellowship to the first author. Additional funding is provided by the *Constellation University Institutes Program*, under NASA grant NCC3-989. The authors would also like to thank Mr. Adam J. Amar of *NASA Johnson Space Center* and formerly from *Sandia National Labs*, for numerous insightful discussions.

References

- ¹Amar, A. J., Blackwell, B. F., and Edward, J. R., "One-Dimensional Ablation Using a Full Newton's Method and Finite Control Volume Procedure," *9th AIAA/ASME Joint Thermophysics and Heat Transfer Conference*, No. AIAA-2006-2910, San Francisco, California, 5-8 June 2006, p. 26.
- ²Amar, A. J., Blackwell, B. F., and Edward, J. R., "One-Dimensional Ablation with Pyrolysis Gas Flow Using a Full Newton's Method and Finite Control Volume Procedure," *39th AIAA Thermophysics Conference*, No. AIAA-2007-4535, Miami, FL, 25-28 June 2007, p. 41.
- ³Amar, A. J., Blackwell, B. F., and Edwards, J. R., "One-Dimensional Ablation Using a Full Newton's Method and Finite Control Volume Procedure," *Journal of Thermophysics and Heat Transfer*, Vol. 22, No. 1, January 2008, pp. 72–82.
- ⁴Amar, A. J., *Modeling of One-Dimensional Ablation with porous Flow Using Finite Control Volume Procedure*, Master's thesis, North Carolina State University, Raleigh, 2006.
- ⁵Blackwell, B. F. and Hogan, R. E., "One-Dimensional Ablation Using Landau Transformation and Finite Control Volume Procedure," *Journal of Thermophysics and Heat Transfer*, Vol. 8, No. 2, April-June 1994, pp. 282–287.
- ⁶Martin, A. and Boyd, I. D., "Variation of the Thomas algorithm for opposed-border tridiagonal systems of linear equations," *Communications in Numerical Methods in Engineering*, Vol. Submitted, 2008.
- ⁷Kendall, R. M., "Thermochemical Ablation," No. AIAA-1965-642, 1965.
- ⁸Blackwell, B. F., Douglas, R. W., and Wolf, H., "A User's Manual for the Sandia One-Dimensional Direct and Inverse Thermal (SODDIT) Code," Tech. Rep. SAND 85-2478, Sandia National Laboratories, Albuquerque, NM, 1987.
- ⁹Powars, C. A. and Kendall, R. M., *Aerotherm Chemical Equilibrium (ACE) Computer Program - User's Manual*, Aerotherm Corporation, Mountain View, California, May 1969.
- ¹⁰Sutton, K., "An Experimental Study of a carbon-Phenolic Ablation Material," Technical Note D-5930, NASA Langley Research Center, Hampton, VA 23365, 1970.
- ¹¹Wakefield, R. M. and C.Pitts, W., "Analysis of the Heat-Shield Experiment on the Pioneer-Venus Entry Probes," *AIAA 15th Thermophysics Conference*, edited by AIAA, No. AIAA-1980-1494, Snowmas, CO, July 14-16 1980.
- ¹²Chen, Y.-K. and Milos, F. S., "Ablation and Thermal Response Program for Spacecraft Heatshield Analysis," *Journal of Spacecraft and Rockets*, Vol. 36, No. 3, May-June 1999, pp. 475–483.
- ¹³Ahn, H.-K., Park, C., and Sawada, K., "Response of Heatshield Material at Stagnation Point of Pioneer-Venus Probes," *Journal of Thermophysics and Heat Transfer*, Vol. 16, No. 3, July-September 2002, pp. 432–439.
- ¹⁴Zeng, Z. and Grigg, R., "A Criterion for Non-Darcy Flow in Porous Media," *Transport in Porous Media*, Vol. 63, No. 1, 2006, pp. 57–69.
- ¹⁵Ruth, D. and Ma, H., "On the derivation of the Forchheimer equation by means of the averaging theorem," *Transport in Porous Media*, Vol. 7, No. 3, 1992, pp. 255–264.
- ¹⁶Whitaker, S., "Flow in porous media I: A theoretical derivation of Darcy's law," *Transport in Porous Media*, Vol. 1, No. 1, 1986, pp. 3–25.
- ¹⁷Suzuki, T., Sawada, K., Yamada, T., and Inatani, Y., "Experimental and Numerical Study of Pyrolysis Gas Pressure in Ablating Test Piece," *Journal of Thermophysics and Heat Transfer*, Vol. 19, No. 3, July-September 2005, pp. 266–272.
- ¹⁸Yamada, T., Sawada, K., Yamada, T., and Inatani, Y., "Thermal Response of Ablative Test Piece in Arc-Heated Wind Tunnel," *42nd AIAA Aerospace Sciences Meeting and Exhibits*, No. AIAA-2004-341, Reno, NV, January 5-8 2004.
- ¹⁹Suzuki, T., Sawada, K., Yamada, T., and Inatani, Y., "Gas Permeability of Oblique-Layered Carbon-Cloth Ablator," *Journal of Thermophysics and Heat Transfer*, Vol. 18, No. 4, 2004, pp. 548–550.
- ²⁰Ergun, S., "Fluid Flow Through Packed Column," *Chem Eng Prog*, Vol. 48, 1952, pp. 89–94.
- ²¹Ward, J. C., "Turbulent flow in porous media," *Journal of the Hydraulics Division, ASCE*, Vol. 90, No. HY-5, 1964, pp. 1–12.
- ²²Marschall, J. and Milos, F. S., "Gas Permeability of Rigid Fibrous Refractory Insulations," *32nd AIAA Thermophysics Conference*, No. AIAA-1997-2479, Atlanta, GA, June 23-25 1997, p. 11.
- ²³Marschall, J. and Milos, F. S., "Gas Permeability of Rigid Fibrous Refractory Insulations," *Journal of Thermophysics and Heat Transfer*, Vol. 12, No. 4, October-December 1998, pp. 8.
- ²⁴Marschall, J. and Cox, M. E., "Gas Permeability of Lightweight Ceramic Ablators," *Journal of Thermophysics and Heat Transfer*, Vol. 13, No. 3, 1999, pp. 382–384.
- ²⁵Scalabrin, L. C. and Boyd, I. D., "Numerical Simulations of the FIRE-II Convective and Radiative Heating Rates," *39th AIAA Thermophysics Conference*, No. AIAA-2007-4044, Miami, FL, 25 - 28 June 2007, p. 17.
- ²⁶Scalabrin, L. C., *Numerical Simulation of Weakly Ionized Hypersonic Flow Over Reentry Capsules*, Ph.D. thesis, The University of Michigan, 2007.
- ²⁷Scalabrin, L. and Boyd, I. D., "Development of an Unstructured Navier-Stokes Solver for Hypersonic Nonequilibrium Aerothermodynamics," *38th AIAA Thermophysics Conference*, No. AIAA-2005-5203, Toronto, Ontario, June 6-9 2005.

- ²⁸Scalabrin, L. and Boyd, I. D., “Numerical Simulation of Weakly Ionized Hypersonic Flow for Reentry Configurations,” *9th AIAA/ASME Joint Thermophysics and Heat Transfer Conference*, No. AIAA-2006-3773, San Francisco, CA, June 5-8 2006, p. 18.
- ²⁹Wright, M. J., Candler, G. V., and Bose, D., “A Data-Parallel Line Relaxation method for the Navier-Stokes equations,” *AIAA Journal*, Vol. 36, No. 9, September 1998, pp. 1603–1609.
- ³⁰Gnoffo, P. A., “Upwind-Biased, Point-implicit Relaxation Strategies for Viscous Hypersonic Flows,” AIAA-1989-1972-CP, July 1989.
- ³¹Thompson, R. A. and Gnoffo, P. A., “Implementation of a Blowing Boundary Condition in the LAURA Code,” *46th AIAA Aerospace Sciences Meeting and Exhibit*, AIAA-2008-1243, Reno, NV, Jan. 7-10 2008.
- ³²Martinelli, S. and Ruffin, S., “Validation Process for Blowing and Transpiration-Cooling in DPLR,” *39th AIAA Thermophysics Conference*, No. AIAA-2007-4255, 2007, p. 9.
- ³³Emmons, H. W. and Leigh, D. C., “Tabulation of the Blasius Function with Blowing and Suction,” Tech. rep., Ministry of Supply, Aeronautical Research Council, 1954.
- ³⁴Kays and Crawford, *Convective Heat and Mass Transfer*, McGraw-Hill, New York, 3rd ed., 1993.
- ³⁵Kuntz, D., Hassan, B., and Potter, D., “Predictions of Ablating Hypersonic Vehicles Using an Iterative Coupled Fluid/Thermal Approach,” *Journal of Thermophysics and Heat Transfer*, Vol. 15, No. 2, 2001, pp. 129–139.
- ³⁶Godin, D., Trépanier, J.-Y., Reggio, M., Zhang, X., and Camarero, R., “Modelling and Simulation of Nozzle Ablation in High-Voltage Circuit-Breaker,” *Journal of Physics D: Applied Physics*, Vol. 33, No. 20, 2000, pp. 2583–2590.
- ³⁷Godin, D. and Trépanier, J.-Y., “A Robust and Efficient Method for the Computation of Equilibrium Composition in Gaseous Mixtures,” *Plasma Chemistry and Plasma Processing*, Vol. 24, No. 3, September 2004, pp. 447–473.
- ³⁸Martin, A., Reggio, M., and Trépanier, J.-Y., “Numerical solution of axisymmetric multi-species compressible gas flow: Towards improved circuit breaker simulation,” *International Journal of Computational Fluid Dynamics*, Vol. 22, No. 4, April–May 2008, pp. 259–271.
- ³⁹Martin, A., Reggio, M., Trépanier, J.-Y., and Guo, X., “Transient ablation regime in circuit breakers,” *Plasma Science and Technology*, Vol. 9, No. 6, December 2007, pp. 653–656.
- ⁴⁰Cohen, C. B. and Reshotko, E., “Similar Solutions for the Compressible Laminar Boundary Layer with Heat Transfer and Pressure Gradient,” Technical Note 3325, NACA, 1955.
- ⁴¹Bianchi, D., Nasuti, F., Martelli, E., and Onofri, M., “A Numerical Approach for High-Temperature Flows over Ablating Surfaces,” *39th AIAA Thermophysics Conference*, No. AIAA-2007-4537, Miami, FL, June 25-28 2007, p. 11.
- ⁴²Bianchi, D., Martelli, E., Nasuti, F., and Onofri, M., “CFD Study of Isothermal Ablation,” *2nd European Conference for Aerospace Sciences*, EUCASS, 2007, p. 8.
- ⁴³Sullivan, J. M. and Kobayashi, W. S., “Spallation modeling in the Charring Material Thermal Response and Ablation (CMA) computer program,” *22nd AIAA Thermophysics Conference*, edited by AIAA, No. AIAA-1987-1516, 1987, p. 7.